A new Si/TiO_2/Pt p-n junction semiconductor to demonstrate photoelectrochemical CO_2 conversion

Thaís Tasso Guaraldo[1,2*], Juliana Ferreira de Brito[1*], David Wood [2] and Maria Valnice Boldrin Zanoni[1]

[1]UNESP, Chemistry Institute of Araraquara, R. Francisco Degni 55, 14800-060 Araraquara – SP, Brazil
[2]School of Engineering and Computing Sciences, Durham University, South Road, Durham, DH1 3LE, England

Abstract

This work presents a new Si/TiO_2/Pt p-n junction semiconductor prepared by sputtering, chemical vapor deposition (CVD), photolithography and lift-off techniques. XRD, EDS, FE-SEM, diffuse reflectance (DRS) and photocurrent vs potential curves had been used for semiconductor characterization. The material was designed for high porosity and uniformity of both TiO_2 and Pt deposits; both TiO_2 anatase phase formation and Pt presence were confirmed. This semiconductor has a characteristic of high light absorption in the ultraviolet and visible regions. A good photocurrent response for the cathodic region was obtained in a CO_2 saturated solution, confirming electron-hole pair formation and CO_2 electron scavenging. A small Si/TiO_2/Pt electrode (1 x 1 cm) was employed in photoelectrocatalytic CO_2 reduction, forming methanol (0.88 mmol L^{-1}), ethanol (2.60 mmol L^{-1}) and acetone (0.049 mmol L^{-1}) as products. These results had been obtained under the following optimal experimental conditions: 0.1 mol L^{-1} $NaHCO_3$, pH 8 saturated with CO_2, 125 W UV-Vis irradiation and -0.8 V bias potential. A Faradaic efficiency of 96.5% was obtained. Suitable charge transfer mechanisms in the electrode surface, and products formation after CO_2 reduction, are proposed.

Key words: Si/TiO_2/Pt, heterojunction, CO_2 reduction, photoelectrocatalysis

*First coauthor: both first and second authors contributed equally to this work.

Comment [DW1]: Do we need to state the wavelength characteristics of this light?

1 Introduction

The conversion of CO_2 into value added products and/or high-energy content fuel is one of the major goals in the modern world [1]. Among the various possible approaches, photocatalysis [2–6] and photoelectrocatalysis [7–10] have been demonstrated as promising, mainly because these techniques have advantages over CO_2 reduction that can be tuned by using different materials as a photocatalyst when combined with light irradiation. This simple arrangement is able to provide electrons and reactive intermediates able to produce several kinds of hydrocarbons, for instance [11,12]. The photoelectrocatalytic method is based on the use of a semiconductor irradiated by light, whose energy is greater than or equal tothat of the band gap, and simultaneously biased by a gradient potential.

Copper and copper oxides [11–19] are the most known widely known p-type semiconductor used for CO_2 reduction, but these suffer from a lack of stability. From this some groups have presented the combination of metals and oxides for robust materials. Cheng et al. [20] employed Pt-modified reduced graphene oxide for photoelectrocatalytic CO_2 reduction. Yang et al. [21] performed photoelectrocatalytic CO_2 reduction using one-dimensional ribbon CoPc enhanced Fe_2O_3 nanotubes, and Li and coworkers [22] prepared TiO_2 nanotubes modified with a CdSeTe nanosheet aiming at photoelectrocatalytic CO_2 reduction.

The semiconductor silicon has theinteresting properties of mechanical strength, high thermal conductivity, a wide electrical conductivity range and, for the purposes of this work, versatile optical characteristics [23]. However, this material has poor chemical stability and can be easily oxidized in aqueous solution under applied potential [24–27].

Comment [DW2]: These materials are not semiconductors – do you mean CuO on Si, for instance?

Comment [DW3]: Ref 23 needs a specific page reference to these claims. Otherwise leave it out – most people know this about silicon, anyway.

Nevertheless, the stability and unusual electrocatalytic properties can be obtained with a composite anode based on a TiO_2 and Si heterojunction [27,28]. P-n semiconductors heterojunctions have been explored previously as photoactive materials for photocatalytic applications [29,30]. This strategy can usually perform an efficient visible-light absorption and improve charge separation efficiency, leading to photocatalytic activity enhancement. These features demonstrate great potential for photoelectrochemical purposes. In agreement with the literature [25] for a n-Si/n-TiO_2 heterojunction, the photogenerated holes under positive bias potential move toward the n-TiO2/electrolyte interface where oxidation reaction takes place. Therefore, the photogenerated electrons in the n-Si move to the counter electrode, where the reduction reaction takes place. For p-Si/n-TiO2 junctions, the flow of electrons and holes at the junction occurs in the opposite direction, generating a smaller photoanodic current density.

Christensen et al [27] has demonstrated that a composite anode based on TiO_2 and Si heterojunction coupled to metal grid (n-Si/TiO_2/Au) has great potential as a photoanode, where holes generated in the n-Si layer can be accelerated to the surface of the TiO_2 by a bias potential. The metal grid combination with a bias potential facilitated the transport of holes from the Si to the TiO_2 surface, and the spill over from the TiO_2 to the metal grid, culminating in the generation of active chemical species at the semiconductor surface [27]. The semiconductor heterojunction of p-Si/TiO_2 has different band bending properties near the junction [25], which enhances the charge separation and minimize recombination within the material. This behavior enhances the possibility of increasing electrons flow at the material semiconductor surface.

Consequently, it could be a good option to promote photoreduction addressed to CO_2 conversion for instance.

TiO_2 band gap engineering has been reported in the literature for CO_2 photocatalytic conversion. TiO_2/SiO_2 and Ru doped, Pt-TiO_2/glass bead and Pt/TiO_2 nanotubes supported photocatalysts are reported by Liu and collaborators for CO_2 conversion [31]. However, Si/TiO_2/Pt photocathode for photoelectrochemical carbon dioxide conversion has not been referenced. Additionally, a small number of materials are described for photoelectrocaytic CO_2 reduction.

The present work investigates the development of a novel composite cathode Si/TiO_2/Pt p-n junction semiconductor prepared by sputtering, CVD and photolithography techniques and its application on the photoelectrocatalytic CO_2 conversion, aiming to generated products with high added value, such as ethanol.

2 Experimental

2.1 Preparation of the new p-n junction Si/TiO_2/Pt electrode

The composite p-Si/TiO_2/Pt electrodes was obtained by using the following procedures [27]. Firstly, the p-type Si wafer substrate (2.0 inches, university wafers) was carefully cleaned in a H_2O_2:H_2SO_4 (1:1) solution during 30 min, washed with deionized water and treated during 2 min in HF:H_2O (1:10) solution with the aim of removing the native SiO_2 layer from the wafer surface. Afterwards the wafer was rinsed in deionized water, and a TiO_2 layer (120 nm) was deposited by sputtering (Moorfield Minilab 3 sputtering system). Argon was used as the sputtering gas, the target was TiO_2 and the pressure was maintained at 2 mT during deposition at room temperature.

Comment [DW4]: Are you sure the wafers were p-type? We received p-type by mistake, and later on realized this is what they were. We then used n-type for the rest of Thais' work with us. I also note from the Brazilian MRS conference paper of last year the substrates were n-type. Did Thais take some p-type wafers to use with you?

The wafer was then annealed at 450 ^{o}C for 30 min under N_2 flow. The back contact was composed of a Au/Sb layer (200 nm) alloyed at 400^{o}C for 15 min and a further Au layer (100 nm), both deposited by e-beam evaporation. Two different photoresists (SF9 and SPR350) were spin coated on the TiO_2 surface and baked. The wafer was then placed in a mask aligner for to expose the pattern for the grid electrode. The pattern was developed in a solution of MF319 developer, and the wafer given a further bake. A Ti seed layer (10 nm) was e-beam deposited for better grid adhesion, followed by a 120 nmPt grid layer. The grid was produced by lifting off the photoresist in NMP, followed by final rinsing in acetone, isopropanol and deionized water.

2.2 Characterization of the new p-n junction Si/TiO_2/Pt electrode

The new p-n junction Si/TiO_2/Pt was characterized by X-ray diffraction recorded on a Siemens Model D 5000 diffractometer. The structures and morphologies were analyzed by field emission scanning electron microscopy (FE-SEM) on a Zeiss model Supra 35 equipped with an energy dispersive X-ray (EDX) spectrometer. Diffuse reflectance spectroscopy was performed in both the infrared and visible regions. Linear sweep voltammetry was carried out at 0.01 V s^{-1} scan rate, in the absence and presence of UV–vis radiation in 0.1 mol L^{-1} sodium bicarbonate solution as supporting electrolyte, with the supporting electrolyte saturated with CO_2.

2.3 Apparatus and procedure for photoelectrochemical CO_2 reduction

The photoelectrocatalytic CO_2 reduction experiments were performed in a cylindrical two-compartment glass reactor equipped with a cooling system. The sample of p-Si/TiO_2/Pt (1 x 1 cm) was inserted in one compartment of the photoelectrocatalytic

Comment [DW5]: As for DW4, is this p- or n-type?

reactor (400 mL) as a working electrode with a saturated Ag/AgCl (KCl sat) electrode as the reference. The working electrode was irradiated by a commercial 125 W UV–Vis light with irradiance of 21 mW cm^{-2} without the bulb vertically inserted in a central quartz bulb. A Pt gauze counter electrode (2 x 2 cm) was inserted in the other photoelectrocatalytic compartment. Controlled-potential electrolysis was carried out using a potentiostat Autolab model PGSTAT 302 under a controlled potential of -0.8 V. The photoelectrocatalytic treatment was carried out for dissolved CO_2 gas (OXI-MEDIN) at room temperature in 0.1 mol L^{-1} $NaHCO_3$ as the supporting electrolyte. Aliquots of were taken at controlled times and products evaluated.

Comment [DW6]: Insert 'the solution'?

2.4 Product profiles in photoelectrochemical CO_2 reduction

Methanol (CH_3OH), ethanol (C_2H_5OH) and acetone (CH_3COCH_3) were analyzed by gas chromatography on a Model CG-2010 Schimadzu instrument coupled with a flame ionization detector employing the solid-phase micro-extraction technique (SPME) [11]. For this purpose, a 0.5 mL aliquot of the photoelectrolyzed solution was transferred to a sealed container (1.5 mL) and submitted to a heated bath for 7 min at 65 ^oC. After this time, the fiber was exposed to the container vapors for 5 min and the vapors injected into the gas chromatograph. The chromatographic column employed was Stabilvax RESTEC 30 m length, 0.25 mm internal diameter and 25 mm film thickness. Nitrogen was used as carrier gas ata 1.0 mL min^{-1} flow rate. The injector was maintained at 250 °C and the detector at 260 °C in the splitless mode. The heating ramp used is as follows: 35 °C for 4 min, 45 °C at 2 °C min^{-1}, 120 °C at 30 °C min^{-1} and 120 °C for 3 min. Analytical curves were constructed and linear relationship was obtained for acetone in the range of 0.5 µmolL^{-1} to 0.1 mmol L^{-1}, with 0.01 to 10.0 mmol

Comment [DW7]: Which fiber?

L^{-1} for methanol and 0.05 to 7.5 mmol L^{-1} for ethanol. The determination coefficients and quantification limits were 0.9854 and 0.05 µmol L^{-1} for acetone, 0.9971 and 0.1 mmol L^{-1} for methanol, 0.9856 and 0.05 mmol L^{-1} for ethanol, respectively.

3 Results and discussions

3.1 p-n Si/TiO_2/Pt semiconductor features

Figure 1a illustrates the top view FE-SEM image obtained for the TiO_2/Pt interface of the p-n Si/TiO_2/Pt semiconductor prepared in this study. The presence of Pt and TiO_2 in the semiconductor interface was confirmed by the EDS analysis (Figure1b). The preparation route led to two different areas, as can be observed in Figure 1a. The left side of the image corresponds to the Pt nanoparticulated area, proven by the EDS results presented in Figure 2b. A FE-SEM image of the main Pt area is shown in Figure 2a. The right area of the Figure 1a image is relative to TiO_2 nanoparticles deposition, which can be confirmed by FE-SEM micrographs and EDS analysis in Figure 3.

Material crystallinity was confirmed by XRD (Figure 4). The diffractogram of the p-n junction Si/TiO_2/Pt semiconductor shows three defined peaks. The peak $2\theta = 25^0$ is relative to the TiO_2 anatase phase, the most photoactive phase of this oxide [32]. The peak $2\theta = 43^0$ is attributed to Pt, and $2\theta = 70^0$ relative to Si. The substrate line in Figure 4 show the peak for Si without modification ($2\theta = 70^0$) which was suppressed after the TiO_2 and Pt depositions.

3.2 Si/TiO2/Pt behavior under UV-Vis irradiation and effect of CO_2 in the photocurrent/voltage curves

Diffuse reflectance analysis was conducted for a standard Si substrate and for the p-n junction Si/TiO_2/Pt, for evaluation of the semiconductor behavior upon UV-Vis irradiation (Figure 5a). The Si substrate presents high values of optical absorption (dashed curve) in all spectra (200 to 800 nm) mainly in the ultraviolet region. However, deposition of TiO_2 and Pt on the substrate causes an increase in optical absorption in the visible region, with two bands around 400 nm and 500 nm, maintaining higher optical absorption in the ultraviolet regions (≤ 380 nm). This behavior indicates that the material shows excellent optical properties and could absorb light over a wide spectrum.

Comment [DW8]: In Figure 5a, lines I and II are not defined in the figure caption.

The inset in Fig. 5(a) shows the Tauc's graph [33] used to estimate the bandgap energy of the material. The diffuse reflectance measurements were converted to an equivalent absorption coefficient by Kubelka-Munk equation:

$$\alpha = (1 - R)^{1/\gamma}/2R \quad (1)$$

Where α is the material absorptivity, R is the reflectance and γ is the power coefficient, which can assume the values 1/2, 3/2, 2 or 3 according to the electronic transition type: direct allowed, direct forbidden, indirect allowed and indirect forbidden, respectively [34,35]. More accurate results in the case of TiO_2 semiconductor are obtained considering the indirect allowed transition (γ = 2) [36]. The p-n junction Si/TiO_2/Pt revealed a band gap value of 2.75 eV as presented in the inset of Figure 5a. The commonly reported band gap value for TiO_2 anatase is 3.2 eV [37–39]. The difference between the TiO_2 anatase and Si/TiO_2/Pt band gap values can be attributed to doping of the TiO_2 with Pt, which introduces an intragap energy level inside the TiO_2

band gap [40]. This behavior contributes to the absorption threshold of ultraviolet towards visible, in addition to a reduction of the material band gap [40].

Figure 5b shows typical photocurrent *vs*. potential curves obtained for a $Si/TiO_2/Pt$ semiconductor in 0.1 mol L^{-1} $NaHCO_3$ solution in dark conditions (I) and irradiated by UV-Vis light before (II) and after (III) saturation with CO_2. A shift towards a less negative potential is observed when the semiconductor is activated by light, indicating that electrons and holes pairs (e^-/h^+) are created inside both Si and TiO_2 due to irradiation in UV-Vis region. The TiO_2 is activated by the UV light and visible light can be harvested by the Si [25]. The photogenerated electrons moves toward the Pt/electrolyte interface [27], where water reduction can takes place to generate hydrogen [21,41].

Figure 6 illustrates the process. In the presence of CO_2 the curve leads to a larger negative onset potential (from -1 to -0.5 V vs Ag/AgCl), indicating the p-n junction promotes more effective separation of photogenerated charges. This indicates that the flat band potential of the semiconductor is lower than the hydrogen reduction potential and CO_2 could be attracted to the $Si/TiO_2/Pt$ surface, but requires an external bias potential higher than -0.4 V (Curve III, Figure 5b). This fact indicates that CO_2 acts as much better electron scavenger (capturing the photoelectrons generated by e^-/h^+ separation from $Si/TiO_2/Pt$) than water [22,41]. $Si/TiO_2/Pt$ under CO_2, light and -0.8 V potential conditions produces a current 5 times higher than the semiconductor without CO_2 and light application, and 3 times more intense than under light without CO_2 saturation. Based on this results, this condition (-0.8 V) was chosen for

photoelectrocatalytic CO_2 reduction experiments, a potential considerably smaller than the thermodynamic potential (vs NHE) necessary for the CO_2 reduction [42].

The photoactivity results suggested that p-n heterojunction Si/TiO_2/Pt electrode acts as very efficient cathode under negative bias potential. The charge transfer mechanism proposed for Si/TiO_2/Pt p-n heterojunction presented in Figure 6 was proposed based in the research of Hwang and coworkers [25], where the electrons generated by a negative bias potential and light incidence in both surfaces, Si and TiO_2, move to lower energy levels and are consequently trapped by the Pt due to a lower Fermi level. The opposite behavior occurs for holes formed at the semiconductor surface. Therefore, electrons move from the counter electrode towards the working electrod,e while holes are generated at the photocathode and reach the Pt counter electrode in order to undertake oxidation reactions. Under negative bias, electron/hole pair recombination is minimized by more efficient charge separation, favoring photoelectrocatalysis target [34,43]. The CO_2 reduction occurs at the Pt surface, where it is converted to $\bullet CO_2^-$ [6,44–46] and hence protonation and deprotonation reactions occur to form the products [12,47]. The overall charge transfer mechanism characterizes the p-n junction [48].

3.3 Photoelectrochemical CO_2 conversion

The photoelectrocatalytic CO_2 conversion in methanol, ethanol and acetone were monitored during 90 min of photoelectrolysis on a Si/TiO_2/Pt electrode in 0.1 mol L^{-1} $NaHCO_3$ saturated with CO_2 (Figure 7a) under a bias potential of -0.80 V and UV-Vis irradiation. The first 30 min of reaction led to the formation of 0.23 mmol L^{-1} of methanol, 0.72 mmol L^{-1} of ethanol and 0.025 mmol L^{-1} of acetone. After 60 min, all the products

formation increased, reaching maximum values at 90 min of reaction with 0.88 mmol L^{-1} of methanol, 2.60 mmol L^{-1} of ethanol and 0.049 mmol L^{-1} of acetone. This is a different result than has been observed in the literature, e.g. [21,22,41,49], where methanol was not generated in the same quantities under these conditions; however, ethanol was, like in our results, the primary product. A faradaic efficiency of 96.5% was obtained after 90 min of photoelectrocatalytic reduction, found by considering the number of electrons necessary for methanol, ethanol and acetone formation by the following reactions:

$$CO_2 + 6e^- + 6H^+ \rightleftarrows CH_3OH + H_2O \quad (1)$$

$$CO_2 + 12e^- + 12H^+ \rightleftarrows C_2H_5OH + H_2O \quad (2)$$

$$CO_2 + 16e^- + 16H^+ \rightleftarrows CH_3COCH_3 + H_2O \quad (3)$$

The efficiency of photoelectrocatalytic reduction ($Si/TiO_2/Pt$, UV-Vis irradiation and -0.80 V) in relation to photocatalysis ($Si/TiO_2/Pt$ and UV-Vis irradiation) and electrolysis ($Si/TiO_2/Pt$ and -0.80 V) was compared by monitoring the CO_2 reduction during 90 min in 0.1 mol L^{-1} $NaHCO_3$ solution, pH 8, saturated with CO_2, by measuring the formation of methanol, ethanol and acetone. Both experiments were able to form only a small amount of acetone as presented in the insert of the Figure 7b. This comparison confirms CO_2 conversion was more effective under UV-Vis irradiation and bias potential.

The mechanism proposed for methanol, ethanol and acetone formation from photoelectrocatalytic CO_2 reduction applied to a p-n junction $Si/TiO_2/Pt$ semiconductor is presented in Figure 8. The mechanism is proposed in agreement with the literature [21,42,50,51], and is based on e^- and $H^\bullet$ transfer. Latest is generated by water oxidation by the holes at the counter electrode [12,17]. The possible reaction shows two different

Comment [DW9]: I'm not sure what this sentence means.

pathways; one of them driving to ethanol formation, and the other to acetone. There is probably one preferential pathway in this case, and this fact can explain the dominant formation of ethanol and the small amount of acetone. The methanol could be considered as a sacrificial product that needs to be formed initially for further ethanol or acetone generation.

4 Conclusion

A new and efficient p-n junction Si/TiO_2/Pt semiconductor was constructed based on the heterojunction benefits using lift off and photolithography techniques. The material obtained presents high porosity of both TiO_2 and Pt deposits, in addition to high light absorption in ultraviolet and visible region. Photocurrent vs potential curves showed a characteristic behavior of a p-n junction semiconductor with a good response in the presence of light and CO_2, proving that semiconductor presents highly efficient electron-hole pairs separation and the CO_2 is a more preferential electron scavenger than water. A small Si/TiO_2/Pt electrode (1 cm^2) was applied in the CO_2 photoelectrocatalytic reduction, confirming the novel electrode is a promising material for photoelectrochemical reduction purposes. The obtained results showed good performance for methanol (0.88 mmol L^{-1}), ethanol (2.60 mmol L^{-1}) and acetone (0.049 mmol L^{-1}) formation as products, presenting 96% of faradaic efficiency. These results were obtained under the best experimental conditions: 0.1 mol L^{-1} $NaHCO_3$, pH 8, saturated with CO_2, 125 W UV-Vis light and -0.8 V. Mechanisms of charge transfer at the electrode surface and for products formation have been proposed in order to clarify how the reactions occur.

5 Acknowledgment

The authors would like to acknowledge Dra. Angela Regina Araújo e Carolina Rabal Biasetto for helpful discussions, and Fapesp (2012/11141-1) and (2013/25343-8) for financial support.

6 References

[1] S. Hangx, Behaviour of the CO_2-H_2O system and preliminary mineralisation model and experiments, CATO Work. WP. 1 (2005) 1–43.

[2] O.K. Varghese, M. Paulose, T.J. Latempa, C.A. Grimes, Nano Lett. 9 (2009) 731–737.

[3] S. Qin, F. Xin, Y. Liu, X. Yin, W. Ma, J. Colloid Interface Sci. 356 (2011) 257–61.

[4] Slamet, H.W. Nasution, E. Purnama, S. Kosela, J. Gunlazuardi, Catal. Commun. 6 (2005) 313–319.

[5] Y. Yuan, Z. Yu, J. Zhang, Z. Zou, Dalton Trans. 41 (2012) 9594–9597.

[6] C. Wang, X. Ma, J. Li, L. Xu, F. Zhang, J. Mol. Catal. A Chem. 364 (2012) 108–114.

[7] B. Aurian-Blajeni, I. Taniguchi, J.O. Bockris, J. Electroanal. Chem. 149 (1983) 291–293.

[8] M. Halmann, Nature. 275 (1978) 15–16.

[9] B.R. Eggins, J.T.S. Irvine, E.P. Murphy, J. Grimshaw, J. Chem. Soc. Chem. Commun. 16 (1988) 1988.

[10] T. Inoue, A. Fujishima, S. Konishi, K. Honda, Nature. 277 (1979) 637–638.

[11] J.F. Brito, A.A. Silva, A.J. Cavalheiro, M.V.B. Zanoni, Int. J. Electrochem. Sci. 9 (2014) 5961–5973.

[12] J.F. Brito, A.R. Araujo, K. Rajeshwar, M.V.B. Zanoni, Chem. Eng. J. 264 (2015) 302–309.

[13] S. Ohya, S. Kaneco, H. Katsumata, T. Suzuki, K. Ohta, Catal. Today. 148 (2009) 329–334.

[14] C.W. Li, M.W. Kanan, J. Am. Chem. Soc. 134 (2012) 7231–4.

[15] Y. Terunuma, a. Saitoh, Y. Momose, J. Electroanal. Chem. 434 (1997) 69–75.

[16] Y. Momose, K. Sato, O. Ohno, Surf. Interface Anal. 34 (2002) 615–618.

[17] K.P. Kuhl, E.R. Cave, D.N. Abram, T.F. Jaramillo, Energy Environ. Sci. 5 (2012) 7050.

[18] K. Rajeshwar, N.R. De Tacconi, G. Ghadimkhani, W. Chanmanee, C. Janáky, ChemPhysChem. 14 (2013) 2251–2259.

[19] W. Siripala, A. Ivanovskaya, T.F. Jaramillo, S.H. Baeck, E.W. McFarland, Sol. Energy Mater. Sol. Cells. 77 (2003) 229–237.

[20] J. Cheng, M. Zhang, G. Wu, X. Wang, J. Zhou, K. Cen, Environ. Sci. Technol. 48 (2014) 7076–7084.

[21] Z. Yang, J. Xu, C. Wu, H. Jing, P. Li, H. Yin, Appl. Catal. B Environ. 156-157 (2014) 249–256.

[22] P. Li, J. Zhang, H. Wang, H. Jing, J. Xu, X. Sui, H. Hu, H. Yin, Catal. Sci. Technol. 4 (2014) 1070.

[23] M.J. Madou, Fundamentals of microfabrication and nanotechnology, third ed., Boca Raton: CRC, 2012.

[24] S.Y. Noh, K. Sun, C. Choi, M. Niu, M. Yang, K. Xu, S. Jun, D. Wang, Nano Energy. 2 (2013) 351–360.

[25] Y.J. Hwang, A. Boukai, P. Yang, Nano Lett. 9 (2009) 410–415.

[26] H. Yu, S. Chen, X. Quan, H. Zhao, Y. Zhang, Appl. Catal. B Environ. 90 (2009) 242–248.

[27] P.A. Christensen, M.A. Carroll, D. Linares-Moya, D. Molyneux, M.C. Rosamond, D. Wood, J. Phys. Chem. C. 115 (2011) 10777–10783.

[28] P. a Christensen, T. a Egerton, W.F. Lin, P. Meynet, Z.-G. Shao, N.G. Wright, Chem. Commun. (Camb). (2006) 4022–4023.

[29] T. Abe, K. Nagai, Org. Electron. Physics, Mater. Appl. 8 (2007) 262–271.

[30] G. Dai, S. Liu, Y. Liang, T. Luo, Appl. Surf. Sci. 264 (2013) 157–161.

[31] G. Liu, N. Hoivik, K. Wang, H. Jakobsen, Sol. Energy Mater. Sol. Cells. 105 (2012) 53–68.

[32] M.F. Brugnera, K. Rajeshwar, J.C. Cardoso, M.V.B. Zanoni, Chemosphere. 78 (2010) 569–75.

[33] J. Tauc, R. Grigorovici, A. Vancu, Phys. Status Solidi. 15 (1966) 627–637.

[34] G.G. Bessegato, J.C. Cardoso, M.V.B. Zanoni, Catal. Today. (2015).

[35] G.G. Bessegato, J.C. Cardoso, M.V.B. Zanoni, Catal. Today. (2014).

[36] R. López, R. Gómez, J. Sol-Gel Sci. Technol. 61 (2012) 1–7.

[37] T.T. Guaraldo, T.B. Zanoni, S.I.C. de Torresi, V.R. Gonçales, G.J. Zocolo, D.P. Oliveira, M.V.B. Zanoni, Chemosphere. 91 (2013) 586–93.

[38] L. Jing, B. Xin, F. Yuan, L. Xue, B. Wang, H. Fu, J. Phys. Chem. B. 110 (2006) 17860–17865.

[39] Y. Cai, Y. Ye, Z. Tian, J. Liu, Y. Liu, C. Liang, Phys. Chem. Chem. Phys. 15 (2013) 20203–9.

[40] H. Wang, J.L. Faria, S. Dong, Y. Chang, Mater. Sci. Eng. B. 177 (2012) 913–919.

[41] G. Ghadimkhani, N.R. De Tacconi, W. Chanmanee, C. Janaky, K. Rajeshwar, Chemical Communications, Chem. Commun. 49 (2013) 1297–1299.

[42] M. Tahir, N.S. Amin, Energy Convers. Manag. 76 (2013) 194–214.

[43] T.T. Guaraldo, S.H. Pulcinelli, M.V.B. Zanoni, J. Photochem. Photobiol. A Chem. 217 (2011) 259–266.

[44] S. Ikeda, T. Takagi, K. Ito, Bull. Chem. Soc. Jpn. 60 (1987) 2517–2522.

[45] N.M. Dimitrijevic, B.K. Vijayan, O.G. Poluektov, T. Rajh, K.A. Gray, H. He, P. Zapol, J. Am. Chem. Soc. 133 (2011) 3964–71.

[46] G. Ghadimkhani, N.R. de Tacconi, W. Chanmanee, C. Janaky, K. Rajeshwar, Chem. Commun. (Camb). 49 (2013) 1297–9.

[47] M.M. Halmann, M. Steinberg, Greenhouse gas carbon dioxide mitigation : science and technology, sixth ed., Fla: Lewis Publishers, Boca Raton, 1999.

[48] L.J. Minggu, K.H. Ng, H.A. Kadir, M. Bin Kassim, Ceram. Int. 40 (2014) 16015–16021.

[49] P. Li, J. Xu, H. Jing, C. Wu, H. Peng, J. Lu, H. Yin, Appl. Catal. B Environ. 156-157 (2014) 134–140.

[50] M. Gattrell, N. Gupta, A. Co, J. Electroanal. Chem. 594 (2006) 1–19.

[51] G.K. Ramesha, J.F. Brennecke, P. V. Kamat, ACS Catal. 4 (2014) 3249–3254.

Provide Captions

Figure 1. (a) FE-SEM image and (b) EDS analysis presenting the interface TiO_2-Pt of the Si/TiO_2/Pt semiconductor.

Figure 2. (a) FE-SEM image and (b) EDS analysis of the Si/TiO_2/Pt semiconductor showing the Pt deposit region.

Figure 3. (a) FE-SEM image and (b) EDS analysis of the Si/TiO_2/Pt semiconductor showing the TiO_2 deposit region.

Figure 4: XRD diffractogram of the Si/TiO_2/Pt semiconductor and the Si substrate.

Figure 5. The p-n junction Si/TiO_2/Pt (a) diffuse reflectance analysis with an insert of the material band gap and (b) photocurrent vs. potential under dark (line I), under UV-Vis

light (line II) and under UV-Vis light with supporting electrolyte saturated with CO_2 (line III).

Figure 6. Charge transfer mechanism for the p-n junction Si/TiO_2/Pt semiconductor.

Figure 7. a) CO_2 conversion into the products methanol (CH_3OH), ethanol (C_2H_5OH) and acetone (CH_3COCH_3) in different times and applying photoelectrocatalysis at -0.8 V and 0.1 mol L^{-1} $NaHCO_3$, pH 8, and b) comparison between the photocatalysis, electrocatalysis and photoelectrocatalysis technique under the same conditions.

Figure 8. Mechanism proposed for methanol, ethanol and acetone formation from the photoelectrocatalytic CO_2 reduction applied to the p-n junction Si/TiO_2/Pt semiconductor.

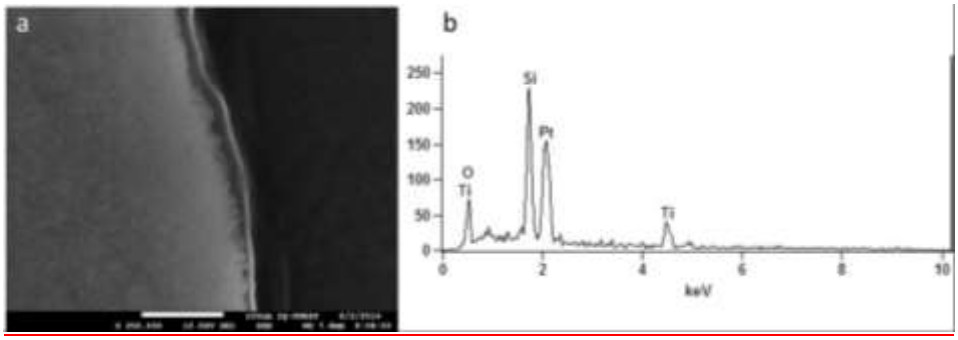

Figure 1.

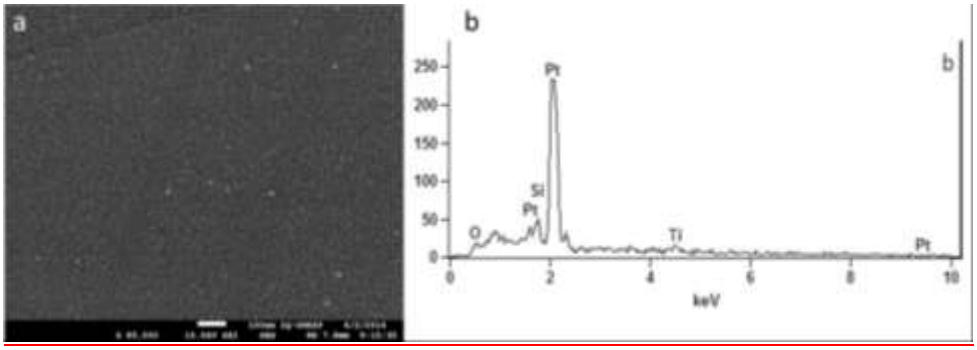

Figure 2.

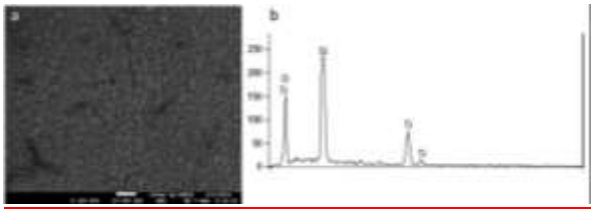

Figure 3.

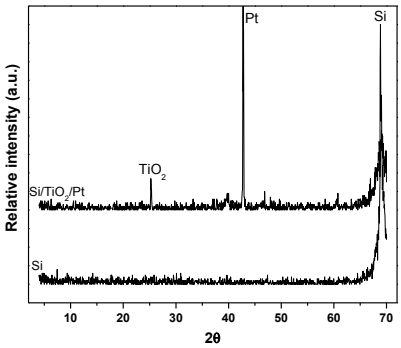

Figure 4.

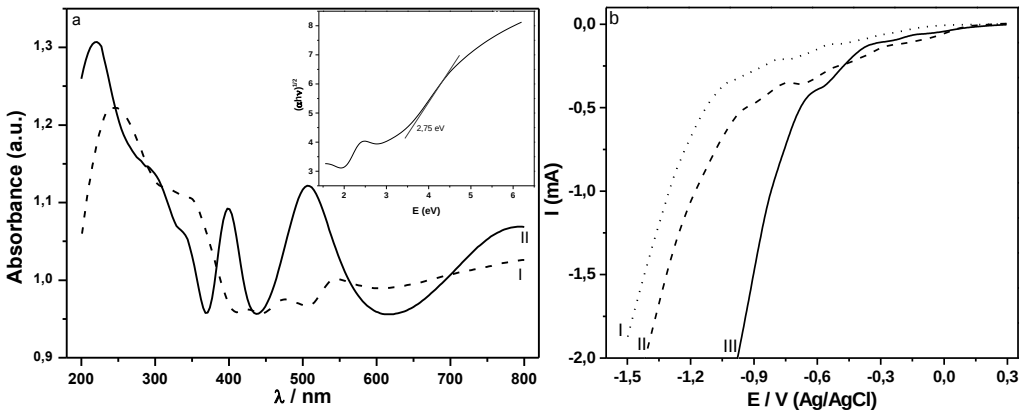

Field Code Changed

Figure 5.

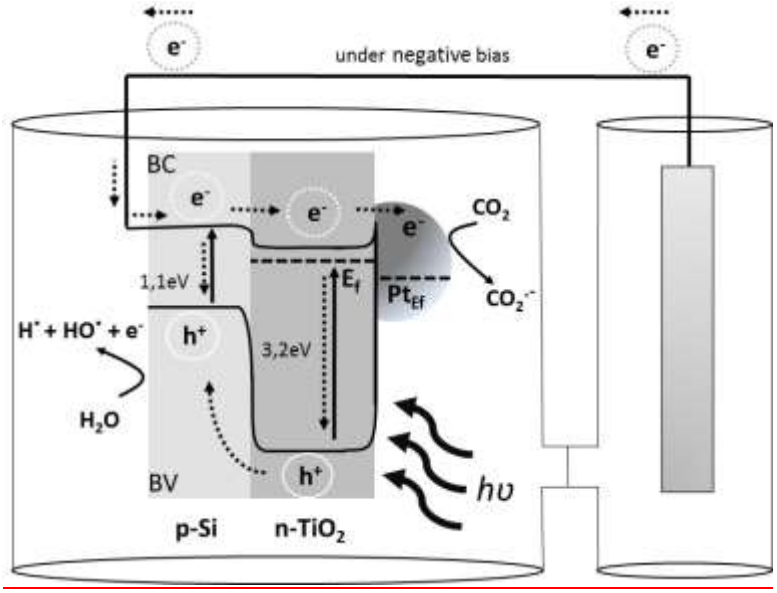

Figure 6.

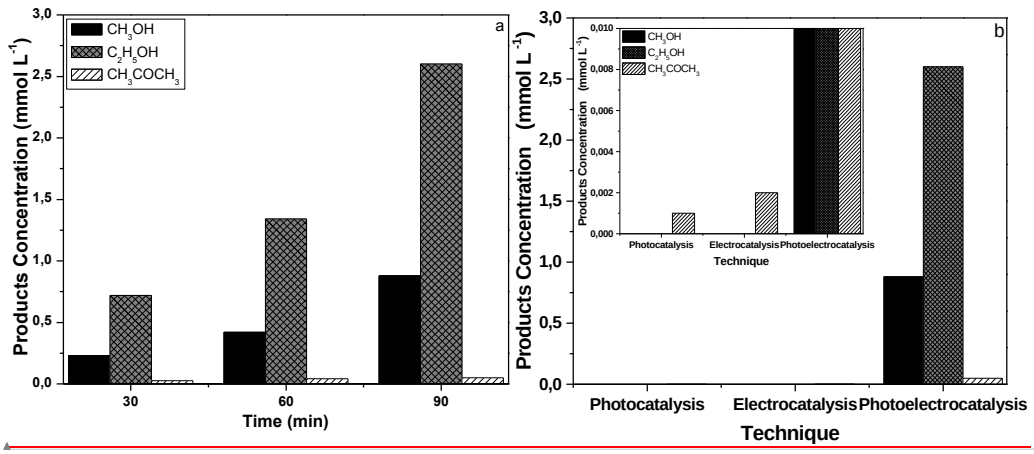

Field Code Changed

Figure 7.

CH_3OH Formation

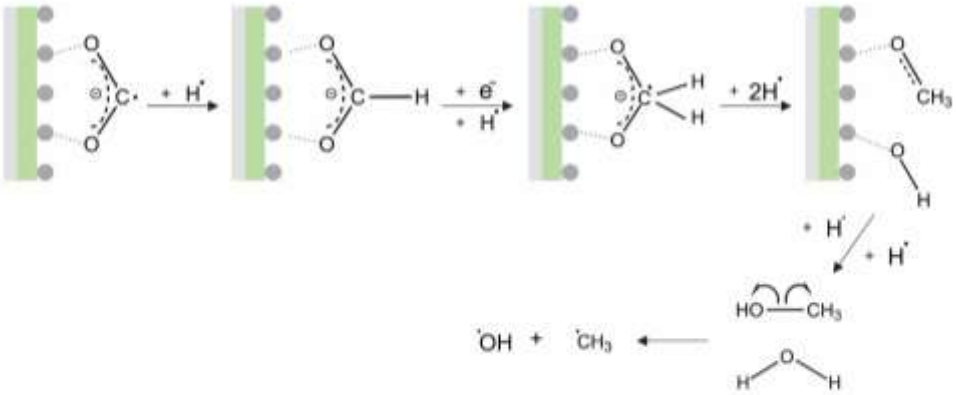

CH_3CH_2OH and CH_3COCH_3 Formation

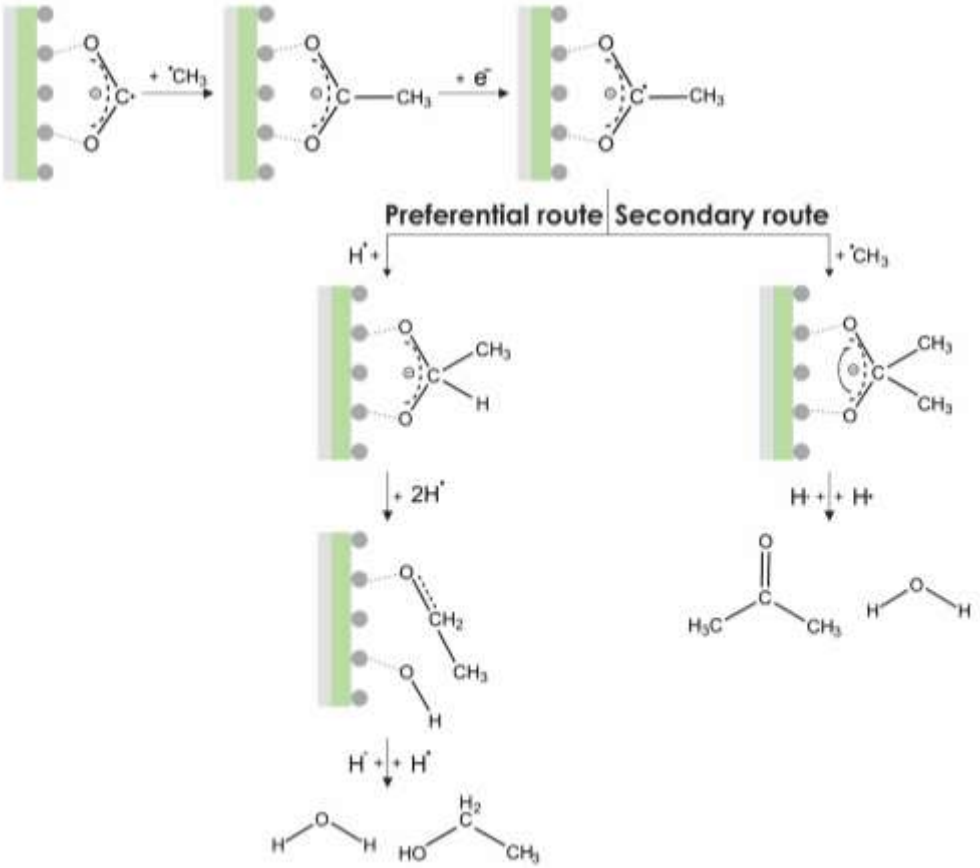

Figure 8.